Theoretical framework for nanoparticle uptake and accumulation kinetics in dividing cell populations

C. Åberg[(a)], J. A. Kim, A. Salvati and K. A. Dawson[(b)]

Centre for BioNano Interactions, School of Chemistry and Chemical Biology, University College Dublin, Belfield, Dublin 4, Ireland

PACS 87.85.Rs – Nanotechnologies-applications
PACS 87.17.Ee – Growth and division
PACS 87.10.Ca – Analytical theories

Abstract – Nano-sized objects interact with biological systems in fundamentally novel ways, thereby holding great promise for targeted drug-delivery. It has also been suggested they could constitute a hitherto unseen hazard. Numerous experimental studies in the field are taking place. We consider that the nature of the interactions allows a more fundamental theoretical framework to be developed. In particular, we describe the intimate link that develops between nanoparticle uptake and cell population evolution. Explicit analytical results are given and the theory compared to experimental observations.

Introduction. – The interactions between nano-sized objects, nanoparticles, and living organisms is currently under intense study [1–12]. The nanoscale is privileged because many endogenous biological processes (for example, internalisation and trafficking of cargoes in cells [13]) operate on the scale of tens of nanometres. Engineered nanoparticles can thereby engage with biological processes in fundamentally new manners [2–4, 14]. In particular, nanoparticles can be directed to, and accumulated in, specific locations within organisms using the cell's energy, unlike small molecules that partition according to basic physicochemical equilibrium principles [15]. These non-equilibrium cell-energy dependent processes are not microscopically reversible, and have suggested a potentially new paradigm of interest for medicines [16–19]. Thus, very small amounts of drugs can be sent to specific locations, rather than rely on the imperfect control of physicochemical properties of molecules to achieve a (quasi-equilibrium) partitioning within the organism, this usually limiting the dose of the medicine that can be delivered.

Nanoparticles associated with the cell surface are imported within small nanoscale capsules (endosomes) and are carried into and within the cell by endogenous cellular processes [20]. Unlike the situation for molecules, there is no reversibility in the transport across the cell membrane. Thus, unless they are specifically recognized for that purpose, nanoparticles are typically not exported out of the cell [1, 15, 21] and accumulate in organelles inside the cell [15, 20, 21]. If the nanoparticles are slow to degrade inside the cell (as many engineered nanoparticles are) they will accumulate until split between daughter cells when the cell divides [1, 15, 22]. Indeed, most cells divide somewhat, even if (as for instance cells in the brain) very slowly. The cells used in laboratories, however, divide rapidly. Cancer cells share this property, leading to unique challenges for therapeutics, for in this case the division of the cells competes with the accumulation of nanoparticles.

Here we show that the absence of equilibration processes, when coupled to ageing and division of individual cells, leads to a predictable history-dependent nanoparticle amount within each cell. In experiments it is possible to measure these amounts individually in great numbers of cells, but more commonly it is the average that is reported, and this has hitherto obscured many of the fundamental details of the processes. We define appropriate ensembles in order to link properties of single cells to their macroscopic averages, and compare to experimental data.

The model. – The time a cell spends between divisions is referred to as the 'cell cycle', and it is divided into four stages ('phases') G_1, S, G_2 and M [fig. 1(a)], of distinct biochemical and morphological activity [23]. In a typical laboratory experiment, many thousands of cells

[(a)] E-mail: Christoffer.Aberg@cbni.ucd.ie
[(b)] E-mail: Kenneth.A.Dawson@cbni.ucd.ie

are asynchronously progressing through this cell cycle in a relatively independent manner. Models of the cell cycle based on reaction networks exist (see *e.g.* ref. [24]), but are not necessary for nanoparticle accumulation studies. We have advanced a simpler model (similar to ref. [25]) that can be solved analytically. Assume that all cells in a population age at the same rate and spend the same amount of time, T, between divisions. If $f(\tau, m, t)\mathrm{d}\tau\mathrm{d}m$ denotes the number of cells of 'age' τ (time elapsed since last division) that contain m nanoparticles, the continuity equation in this space reads

$$\frac{\partial f}{\partial t} + \frac{\partial f}{\partial \tau} + \frac{\partial}{\partial m}\big(J(\tau, m, t) f\big) = 0, \qquad (1)$$

where J is the uptake rate of nanoparticles by cells. We neglect interactions among neighbouring cells and cell death, all reasonable for experiments currently of interest, but these elements could in principle be accommodated. For several nanoparticle/cell systems studied experimentally there is no export of nanoparticles from the cells [1, 15, 21], and the intracellular nanoparticles are split between daughter cells upon division [1, 15, 22]. For such systems $f(\tau, m, t)$ fulfills the boundary condition

$$f(\tau = 0, m, t) = 2 \int f(\tau = T, m', t)\Theta(m', m)\mathrm{d}m', \qquad (2)$$

where $\Theta(m', m)$ is the probability that upon division one of the daughters receives m, if the original cell has m', nanoparticles. Experiments indicate (assuming a binomial distribution) nanoparticle-containing endosomes splitting asymmetrically [22], but below we illustrate with the case of both daughters receiving half of the nanoparticles of the original cell, *i.e.* $\Theta(m', m) = \delta(m - m'/2)$.

Cell cycle. – Equations (1)-(2) is our basic framework that has to be solved for initial conditions of interests. We start by relating and validating the model to experimental observations of cell population growth and cell cycle progression. Thus we ignore cellular nanoparticle amount (for the moment), and let $n(\tau, t) = \int f(\tau, m, t)\mathrm{d}m$ denote the reduced distribution. The total number of cells, $N(t) = \int_0^T n(\tau, t)\mathrm{d}\tau$, grows monotonically and steady-state solutions (with $n(\tau, t)/N(t)$ time independent) have the form $n(\tau, t) = 2\lambda e^{-\lambda\tau} N(t) \equiv 2\lambda e^{-\lambda\tau} N_0 e^{\lambda t}$, where N_0 is the initial total number of cells and $\lambda T = \ln 2$. Steady-state solutions exhibit exponential growth, typical of experimental cell cultures studied in the laboratory. The total duration of the cell cycle, T, can consequently be evaluated experimentally. Figure 1(c) shows the steady-state distribution, from which we observe that the duration of a phase can be related to the fraction of cells in it [26]. The fraction of cells in a phase can be readily measured, and thus all parameters of the cell cycle model can be fixed by experiment. To make explicit connection with experiments, we will in the following use parameters appropriate for A549 (human lung carcinoma) cells in our illustrations of the theory. In this case we have previously

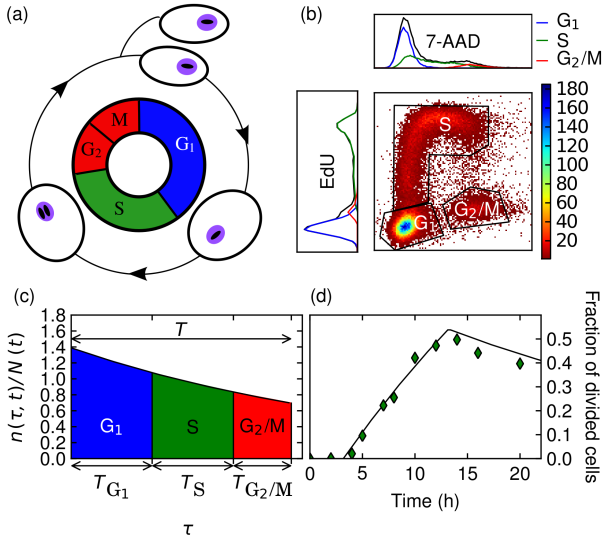

Fig. 1: Results and experimental validation of cell cycle model. (a) Cell progressing through one cell cycle, starting at the beginning of G_1 phase, continuing through S and G_2. During M phase it divides into two daughter cells, starting their respective cycles anew in G_1. (b) Experimental identification of cells in different cell cycle phases. Cells were labelled with two different fluorescent markers (EdU, 5-ethynyl-2′-deoxyuridine, and 7-AAD, 7-aminoactinomycin), and the fluorescence (arbitrary units) of both markers measured in more than 40,000 individual cells using flow cytometry. The colour-map shows the distribution of cells in terms of these two markers, from which cells in G_1, S and G_2/M can be identified as indicated. Resolution between G_2 and M requires more advanced methods and is not necessary for the description given here. See ref. [1] for more details. Insets show the corresponding projections with the contributions of individual phases indicated. (c) Steady-state distribution of cells along the cell cycle. The duration, T_ϕ, of a phase ϕ can be related to the fraction of cells in ϕ, as schematically illustrated for $\phi = G_1$, S and G_2/M. (d) Parameter-free prediction of divided cell fraction compared to corresponding experimental results. Previous simulations [1] produce identical results. Experimental data in panels b and d reproduced from ref. [1].

measured all parameters (see ref. [1] for details); for example, fig. 1(b) shows an experimental determination of the fraction of cells in the different phases.

Having fixed all parameters by experiment, we can validate the model by subsequent parameter-free studies. For our example of A549 cells we have previously measured the fraction of cells that divide with time [1], as shown in fig. 1(d) together with the corresponding theoretical prediction. The striking agreement constitutes a firm basis for the future development of the model to include nanoparticle accumulation. It is noteworthy that considerable efforts have been made experimentally to gather data of high quality to enable such quantitative agreement.

Nanoparticle accumulation inside cells following short-time (pulse) exposure to nanoparticles.

– Having validated the cell cycle part of the model, we continue with the effect the cell cycle has on nanoparticle accumulation. Essentially, our interest concerns how cell-cycle traversal affects the number of nanoparticles per cell, and how to define ensembles useful for experimental comparison. We start with cells exposed to nanoparticles for a limited time (a pulse), short compared to the cell population evolution [fig. 2(a)]. Solutions to eqs. (1)-(2) with zero flux, $J = 0$, naturally show a constant total number of nanoparticles, $M(t) = \iint mf(\tau, m, t)\mathrm{d}m\mathrm{d}\tau$, after nanoparticle exposure. The mean number of nanoparticles per cell, $M(t)/N(t)$, consequently decays exponentially for a cell population growing exponentially.

Experimental studies have reported this seemingly simple exponential decay of the mean amount of nanoparticles per cell, but during the averaging procedure a more complex evolution in terms of individual cell cycle phases is lost. Figure 2(b) shows the nanoparticle amount, $M_\phi(t)/N_\phi(t)$, of cells in the ϕ phase according to the model, assuming all cells initially have the same number, m_0, of nanoparticles. Cells originally in G_2/M divide first, (on average) halving their nanoparticle amount as they restart in G_1. Consequently, the mean nanoparticle amount of G_1 cells decays exponentially. Meanwhile, the mean of S and G_2/M cells remain constant, as cells entering these phases have the original nanoparticle amount. Once *all* G_1 cells are divided cells, the mean nanoparticle amount of G_1 cells remains constant. Subsequently, divided cells with halved nanoparticle amount enters S phase, and the corresponding mean decays exponentially. Finally, divided cells reach the G_2/M phase, with concomitant decay of its mean. The rate of decay depends on the duration of a phase, as in a short phase fewer cells have to be replaced by cells with halved nanoparticle amount. After one cell cycle, all cells have halved their nanoparticle amount, and the process repeats.

The full distribution, $f(\tau, m, t)$, gives a complete theoretical description of the process. Interestingly, $f(\tau, m, t)$ is also essentially experimentally observable, in the sense that we only need to convert the τ-dependence into a dependence on DNA amount (see ref. [27] for details). G_1 and G_2/M cells have, respectively, 'single' and 'double' DNA amount, while S phase cells have amounts in between these two extremes [*cf.* fig. 1(b) top inset]. Figure 2(c) shows this distribution, for the case when both daughter cells receive half of the nanoparticles upon division, using parameters appropriate for the example A549 cells. Initially, all cells have the same nanoparticle amount (left). With time, G_2/M cells divide, forming a subpopulation with single DNA amount and halved nanoparticle amount, while cells originally in G_1 and S progress to S and G_2/M, respectively (centre). Later, all cells originally in G_2/M have divided and all cells originally in G_1 progressed to S (right).

Figure 2(d) shows corresponding experimental distributions as a function of time following a 4 h-exposure of A549 cells to 40 nm (diameter) fluorescently labelled carboxylated polystyrene nanoparticles. Experimentally the initial cellular nanoparticle amount is heterogeneous among cells from the same population (left), which is easily incorporated into the model (see below). However, we also observe the characteristic decay of nanoparticle concentration [fig. 2(d)] as predicted by the model [fig. 2(c)]. The decay of nanoparticle fluorescence is directly correlated to DNA amount, supporting further the idea that

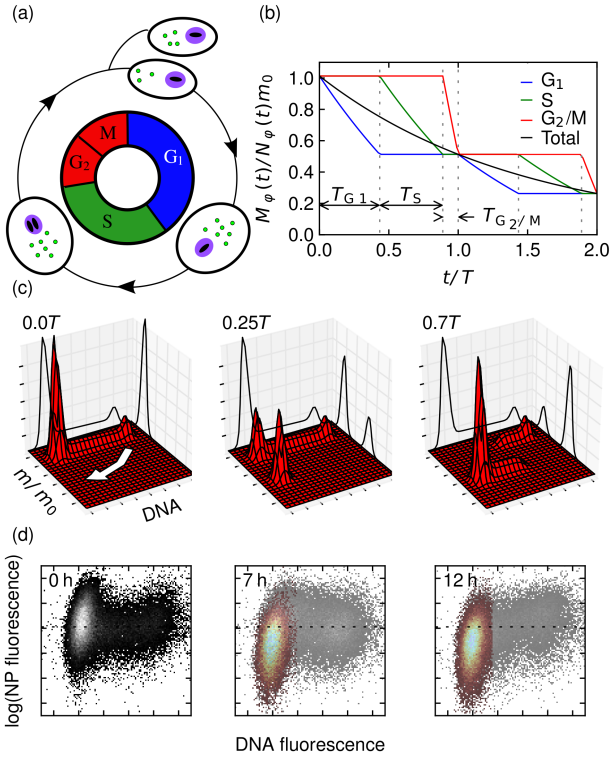

Fig. 2: Evolution of cellular nanoparticle amount in the absence of further nanoparticle uptake. Cells were assumed to originally have identical nanoparticle amounts, imitating cells exposed to a nanoparticle pulse. (a) Cell progressing along the cell cycle, splitting intracellular nanoparticles upon division. No export of nanoparticles from the cell is considered. (b) Evolution of mean nanoparticle amount of cells (instantaneously) in the different phases and the total mean. (c) Normalised distribution of cells in terms of DNA and nanoparticle amount for some representative times. The nanoparticles were assumed to be split evenly between daughter cells and the arrow (left panel) indicates the evolution of cells upon division. The graphs on the coordinate planes show the normalised distribution in DNA and nanoparticle amount, respectively, and δ functions are visualised as Gaussians. Cell cycle parameters in accordance with experiments reproduced in fig. 1. (d) Experimental DNA-nanoparticle fluorescence distributions (in arbitrary units) measured by flow cytometry, reproduced from ref. [1]. The indicated times are counted after the nanoparticle source was removed following a 4 h nanoparticle exposure to cells. Note the log scale in nanoparticle fluorescence. The coloured region corresponds to divided cells and the shaded region is the full population. Dotted line shows mean of the initial (0 h) nanoparticle fluorescence over the full population.

reduction of nanoparticle amount arises from cell division, rather than export out of cells.

Nanoparticle uptake during continuous exposure. – The more usual laboratory experiment involves continuous exposure of cells [fig. 3(a)] to an excess of nanoparticles so that the ambient concentration remains constant. We then have nanoparticle fluxes into cells per unit time, $J(\tau, m, t)$, with the independent variables reflecting biological and other details (*e.g.* the number of receptors, cell surface area and current number of internalised nanoparticles). Current evidence suggests that J is independent of m and t. To investigate uptake rates that are different among cell cycle phases we, however, let $J(\tau)$ depend on the instantaneous phase of the cell, parametrised by τ. The mean nanoparticle amount of the full population (growing exponentially) is then given by $M(t)/N(t) = \overline{M}(t) = \langle J\rangle\big(1 - e^{-\lambda t}\big)/\lambda$ [15]. Here the ensemble-averaged mean uptake rate, $\langle J\rangle = J_{\mathrm{G}_1}u_{\mathrm{G}_1} + J_{\mathrm{S}}u_{\mathrm{S}} + J_{\mathrm{G}_2/\mathrm{M}}u_{\mathrm{G}_2/\mathrm{M}}$, for uptake rates, J_ϕ, that are constant within each phase, ϕ, and u_ϕ is the fraction of cells in ϕ. Again, this development of the theory is formulated such that all parameters are experimentally measurable to facilitate a close connection to experiments.

Figure 3(b) shows that the mean uptake is initially linear (dotted line), while for times comparable to the cell cycle length, uptake competes with reduction of nanoparticle amount due to cell division (solid line). Both observations are corroborated experimentally [1, 15, 21], as exemplified in fig. 3(b) (inset) for A549 cells exposed to 40 nm (diameter) fluorescently labelled carboxylated polystyrene nanoparticles. Asymptotically, one observes a constant mean cellular nanoparticle amount, $\langle J\rangle/\lambda$. Presently there is some uncertainty in the literature as to the origin of the non-linear nanoparticle uptake kinetics; we believe that, typically, rather than competition between nanoparticle uptake and export leading to a steady state, one is observing the mechanism described here.

The mean intracellular nanoparticle amount of individual phases, $M_\phi(t)/N_\phi(t)$, exhibits more complex behaviour. Depending on the nanoparticle uptake rates during individual phases, J_ϕ, the behaviour can vary greatly, as shown in fig. 3(c) for some example sets of rates and with cell cycle parameters appropriate for A549 cells. If the cellular impact of nanoparticles is related to the intracellular nanoparticle concentration, then these different accumulations can have many practical outcomes, yet to be analysed. For the case of A549 cells exposed to 40 nm (diameter) fluorescently labelled carboxylated polystyrene nanoparticles, the uptake rates are roughly independent of phase. The theory [fig. 3(c) left] then predicts that the cellular nanoparticle amount is ranked: $\mathrm{G}_2/\mathrm{M} > \mathrm{S} > \mathrm{G}_1$, an observation that is indeed validated by experiments on these cells [1].

The full distribution, $f(\tau, m, t)$, gives the complete picture, in essence carrying the complete history of nanoparticle accumulation and cell division. To have an illustration

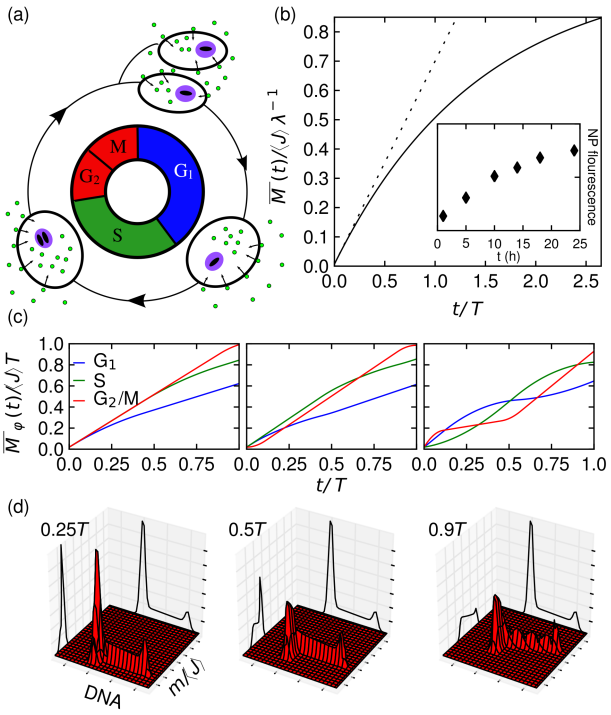

Fig. 3: Evolution of cellular nanoparticle amount during continuous exposure to nanoparticles. (a) Cell progressing along the cell cycle while taking up nanoparticles throughout all phases, splitting its intracellular nanoparticles upon division. No export of nanoparticles from the cell is considered. (b) Mean nanoparticle amount for a cell population growing exponentially. Solid line: full result. Dotted line: linear approximation valid for short times. Inset: corresponding mean nanoparticle fluorescence measured experimentally, reproduced from ref. [1]. (c) Prediction of the effect of different uptake rates on the mean nanoparticle amount of cells that are, in that moment, in the different phases. Left: phase-independent uptake rates. Centre: uptake rates, J_{G_1}:J_{S}:$J_{\mathrm{G}_2/\mathrm{M}}$, in proportion 100:100:1. Right: 5:1:10. Previous simulations [1] produce identical results. (d) Normalised distribution of cells in terms of DNA and nanoparticle amount for some representative times. The nanoparticles were assumed to be split evenly between daughters upon division. The graphs on the coordinate planes show the normalised distribution in DNA and nanoparticle amount, respectively, and δ functions are visualised as Gaussians. Cell cycle parameters in accordance with experiments reproduced in fig. 1 for panels c-d.

that is closer to experiment, we again evaluate this distribution in terms of DNA amount rather than τ. Figure 3(d) shows this distribution for phase-independent uptake rates and both daughter cells receiving half of the intracellular nanoparticles upon division. Cells not yet divided move continuously towards higher nanoparticle amounts, simultaneously reducing in number as cells progressively divide. Divided cells have instead taken up some nanoparticles prior to division and some after; recently divided cells have half, while cells that divided early almost the same, nanoparticle amount as cells not yet divided. After

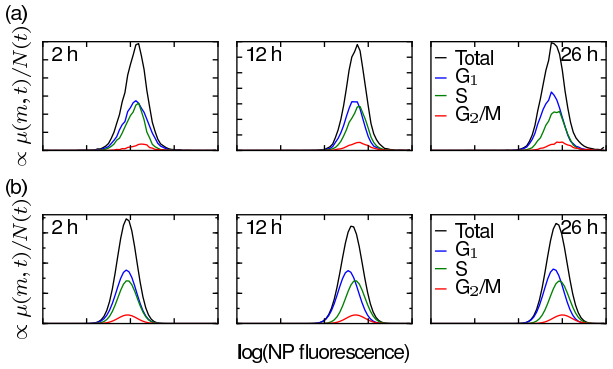

Fig. 4: Cellular nanoparticle amount during continuous nanoparticle uptake, including heterogeneous uptake rates within cell population. Note the log scale in nanoparticle amount. (a) Experimental distribution (in arbitrary units), reproduced from ref. [1]. (b) Results from model, using a log-normal distribution in uptake rates, with scale parameter 0.5 and location parameter adjusted to correspond to experimental measurements. Cell cycle parameters set in accordance with results reproduced in fig. 1. Previous simulations [1] produce identical results.

one full cell cycle, cells are distributed along the interval $[\frac{1}{2}J, J]$ in an exponential fashion, reflecting the underlying age distribution [fig. 1(c)].

For detailed comparisons with experiments, the large heterogeneity in nanoparticle uptake kinetics within the cell population must be taken into account. In the simplest case of phase-independent uptake rates (which is relevant for our previous experiment [1]), we let $f_J(J)$ denote the normalised distribution in rates. For simplicity, we assume that both daughter cells inherit the uptake capacity of the original cell; thus, $f_J(J)$ is time-independent. Uptake rate heterogeneity can be included by integrating previous results with $f_J(J)$ as a kernel, most results remaining valid. As an explicit illustration we compare with our previous experimental results on A549 cells exposed to 40 nm (diameter) fluorescently labelled carboxylated polystyrene nanoparticles [fig. 4(b)] by using cell cycle parameters appropriate for these cells. We, furthermore, utilize a log-normal distribution in uptake as proposed previously [28] and adjust the parameters such that the distribution of nanoparticle amount, $\mu_(m,t) = \int f(\tau, m, t)\mathrm{d}\tau$, of the full population agrees with experiments. Subsequently the theory gives a parameter-free prediction of the distribution of nanoparticle amount in the different cell cycle phases, $\mu_\phi(m,t) = \int f(\tau, m, t)\mathrm{d}\tau$, as shown in fig. 4(a). The striking agreement with the experimental data [fig. 4(b)] suggests that careful experimental studies will be able to recover also the more detailed predictions described above.

Targeting of fast-dividing cells and therapeutics. – We reiterate how different the processing of nanoparticles by cells is compared to small molecules. This will be reflected in optimal choices for nanoparticle-based cancer therapeutics, but interestingly, no theoretical framework has been developed. For small molecules the capacity to equilibrate across the plasma membrane typically ensures rapid equilibration of drug into the cell, even as it is dividing. Nanoparticles have the merit that their trafficking properties are so well regulated by the cell (requiring explicit signals for export) that they accumulate irreversibly. Naturally at some point the drug may be released from its nanoform inside the cell, but this cannot make the situation more favourable (molecules will partition to the outside of the cell) and the basic mechanism of cell division dilutes the intracellular nanoparticle content.

We now have a simple model that is able to quantitatively reproduce nanoparticle accumulation for fast-dividing cells, and can use it to predict and optimise cancer targeting strategies. Naturally there are (*in vivo*) other complicating factors, but the basic understanding derived from the present model yields various insights, not yet appreciated. For cancer-targeting the aim is to achieve a higher dose in fast-dividing (cancerous) cells compared to slow-dividing (healthy) cells. Treating the healthy cells as essentially non-dividing and assuming a linear nanoparticle uptake for them, the targeting efficiency (the ratio of nanoparticle content in cancerous to healthy cells) becomes $\overline{M}_\mathrm{c}(t)/\overline{M}_\mathrm{h}(t) = \langle J\rangle_\mathrm{c}/\langle J\rangle_\mathrm{h}\big(1-e^{-\lambda t}\big)/(\lambda t)$. We might for example target cells in the S, G_2 and/or M phases [1], since non-dividing cells do not pass through these phases. For this case we write $\langle J\rangle_\mathrm{c} = (1-\alpha)\langle J\rangle_\mathrm{h} + \alpha\langle J\rangle_\mathrm{t}$, where α is the fraction of cells in the targeted phases and $\langle J\rangle_\mathrm{t}$ the flux into them. We have assumed (for simplicity) that cells in the remaining phase(s) take up nanoparticles at the same rate as non-dividing cells.

Figure 5a shows the targeting efficiency as a function of time, using parameters (as validated in connection with fig. 1) suitable for targeting S phase A549 cells for definiteness. It is clear that regardless of how large a flux ratio, $\langle J\rangle_\mathrm{t}/\langle J\rangle_\mathrm{h}$, is achieved, eventually the mean dose of the non-dividing cell population exceeds that of the dividing population, an unfavourable outcome from the therapeutic perspective, though of course it is intended that the nanoparticle-carried therapy be released inside the cell at an appropriate time. A relevant time-scale is set by the retention time of nanoparticles in the body (*i.e.*, the time that nanoparticles circulate in the bloodstream and are exposed to the tumour). Figure 5b shows the necessary flux ratios that must be achieved for successful targeting for some realistic nanoparticle retention times. For example, to obtain a ten-fold excess of nanoparticle accumulation in cancer cells during 24 h, a 34 times higher flux into (in this illustration) S phase cells must be achieved. The model places rather concrete bounds on the enhancements of rates of cancer compared to normal cell entry required for a meaningful approach, and can also suggest an ideal time at which the drug should be released inside the cell.

Discussion. – In summary, we emphasise that nanoparticles interacting with cells represent entirely new

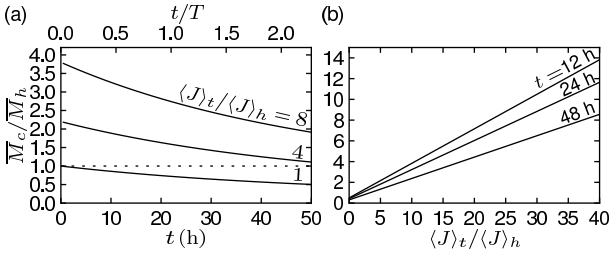

Fig. 5: Prediction of the targeting efficiency for nanoparticle-based cancer therapeutics. Results are presented in terms of the ratio, $\overline{M}_c/\overline{M}_h$, of mean nanoparticle nanoparticle content (dose) in a fast-dividing (cancerous) to a non-dividing (healthy) cell population. Parameters were chosen to correspond to targeting S phase A549 cells (in accordance with results reproduced in fig. 1). (a) Targeting efficiency as a function of exposure time, t. Different curves correspond to different fluxes into cells in the targeted phase. Successful targeting (higher dose in fast-dividing compared to healthy cells) corresponds to $\overline{M}_c/\overline{M}_h > 1$, as indicated by the dotted line. (b) Targeting efficiency as a function of flux-ratio, $\langle J\rangle_t/\langle J\rangle_h$. Different curves correspond to different exposure times to illustrate the effect of different nanoparticle retention times in the body.

systems which can be described theoretically, and will likely be the topic of greatly increased modelling in the coming years. Until now, in the absence of any guiding theoretical framework, the averaging of cellular readouts over inappropriate ensembles has been adopted, without alteration, from small molecule-cell interactions. However, the non-equilibrium uptake of nanoparticles leads to each cell having a history-dependent nanoparticle amount based on its cell cycling. We have shown that in future all cellular effects (based on intracellular concentration) of nanoparticles should be appropriately averaged over the cell-cycle ensembles, and provided the machinery to do so. This would put the whole arena of nanoparticle-cell interactions on a more secure basis, and possibly eliminate current apparent inconsistency in experiments.

* * *

Funding was provided by the Irish Research Council for Science, Engineering and Technology (C.Å.), Science Foundation Ireland (09/RFP/MTR2425) (C.Å.), EU FP7 via the small collaborative project NanoTransKinetics (NMP4-2010-EU-US-266737) (C.Å.) and the INSPIRE programme, funded by the Irish Government's Programme for Research in Third Level Institutions, Cycle 4, National Development Plan 2007-2013 (J.A.K., A.S.). The project is based upon works supported by Science Foundation Ireland (SFI/SRC/B1155), the EU FP7 small collaborative project NeuroNano (NNP4-SL-2008-214547) and the ESF Research Networking Programme EpitopeMap.

REFERENCES

[1] Kim J. A., Åberg C., Salvati A. and Dawson K. A., *Nat. Nanotechnol.*, **7** (2012) 62.
[2] Nel A., Xia T., Mädler L. and Li N., *Sci.*, **311** (2006) 622.
[3] Oberdörster G., Oberdörster E. and Oberdörster J., *Environ. Health Perspect.*, **113** (2005) 823.
[4] Shvedova A. A., Kagan V. E. and Fadeel B., *Annu. Rev. Pharmacol. Toxicol.*, **50** (2010) 63.
[5] Pompa P. P., Vecchio G., Galeone A., Brunetti V., Maiorano G., Sabella S. and Cingolani R., *Nanoscale*, **3** (2011) 2889.
[6] Cedervall T., Lynch I., Lindman S., Berggård T., Thulin E., Nilsson H., Dawson K. A. and Linse S., *Proc. Natl. Acad. Sci. U. S. A.*, **104** (2007) 2050.
[7] Aggarwal P., Hall J. B., McLeland C. B., Dobrovolskaia M. A. and McNeil S. E., *Adv. Drug Deliv. Rev.*, **61** (2009) 428.
[8] Donaldson K., Stone V., Tran C. L., Kreyling W. and Borm P. J. A., *Occup. Environ. Med.*, **61** (2004) 727.
[9] Colvin V. L., *Nat. Biotechnol.*, **21** (2003) 1166.
[10] Handy R. D., Owen R. and Valsami-Jones E., *Ecotoxicol.*, **17** (2008) 315.
[11] Gil P. R., Oberdörster G., Elder A., Puntes V. and Parak W. J., *ACS Nano*, **4** (2010) 5527.
[12] Xia X.-R., Monteiro-Riviere N. A. and Riviere J. E., *Nat. Nanotechnol.*, **5** (2010) 671.
[13] Watson P., Jones A. T. and Stephens D. J., *Adv. Drug Deliv. Rev.*, **57** (2005) 43.
[14] Deng Z. J., Liang M., Monteiro M., Toth I. and Minchin R. F., *Nat. Nanotechnol.*, **6** (2011) 39.
[15] Salvati A., Åberg C., dos Santos T., Varela J., Pinto P., Lynch I. and Dawson K. A., *Nanomedicine*, **7** (2011) 818.
[16] Ferrari M., *Nat. Rev. Cancer*, **5** (2005) 161.
[17] Park J.-H., von Maltzahn G., Xu M. J., Fogal V., Kotamraju V. R., Ruoslahti E., Bhatia S. N. and Sailor M. J., *Proc. Natl. Acad. Sci. U. S. A.*, **107** (2010) 981.
[18] Farokhzad O. C. and Langer R., *ACS Nano*, **3** (2009) 16.
[19] Brigger I., Dubernet C. and Couvreur P., *Adv. Drug Deliv. Rev.*, **54** (2002) 631.
[20] Rejman J., Oberle V., Zuhorn I. S. and Hoekstra D., *Biochem. J.*, **377** (2004) 156.
[21] Shapero K., Fenaroli F., Lynch I., Cottell D. C., Salvati A. and Dawson K. A., *Mol. Biosyst.*, **7** (2011) 371.
[22] Summers H. D., Rees P., Holton M. D., Brown M. R., Chappell S. C., Smith P. J. and Errington R. J., *Nat. Nanotechnol.*, **6** (2011) 170.
[23] Hartwell L. H. and Weinert T. A., *Sci.*, **246** (1989) 629.
[24] Tyson J. J. and Novak B., *Curr. Biol.*, **18** (2008) R759.
[25] Spinelli L., Torricelli A., Ubezio P. and Basse B., *Math. Biosci.*, **202** (2006) 349.
[26] Steel G. G., *Growth Kinetics of Tumors: Cell Population Kinetics in Relation to the Growth and Treatment of Cancer* (Clarendon Press, Oxford) 1977.
[27] Gray J. W., *J. Histochem. Cytochem.*, **22** (1974) 642.
[28] Neti P. V. and Howell R. W., *J. Nucl. Med.*, **47** (2006) 1049.